Structural Basis for a Kolbe−Type Decarboxylation Catalyzed by a Glycyl Radical Enzyme

ARTICLE *in* JOURNAL OF THE AMERICAN CHEMICAL SOCIETY · AUGUST 2011

Impact Factor: 12.11 · DOI: 10.1021/ja203344x · Source: PubMed

JACS
JOURNAL OF THE AMERICAN CHEMICAL SOCIETY

ARTICLE

pubs.acs.org/JACS

Structural Basis for a Kolbe-Type Decarboxylation Catalyzed by a Glycyl Radical Enzyme

Berta M. Martins,*[,†] Martin Blaser,[‡,§] Mikolaj Feliks,[∥] G. Matthias Ullmann,[∥] Wolfgang Buckel,[‡,§] and Thorsten Selmer[‡,⊥]

[†]Institute für Biologie, Strukturbiologie/Biochemie, Humboldt-Universität zu Berlin, D-10115 Berlin, Germany

[‡]Laboratorium für Mikrobiologie, FB Biologie, Philipps-Universität, D-35032 Marburg, Germany

[§]Max-Planck-Institut für Terrestrische Mikrobiologie, D-35043 Marburg, Germany

[∥]Structural Biology/Bioinformatics, Universität Bayreuth, D-95440 Bayreuth, Germany

[⊥]AG Biotechnologie/Enzymtechnologie, Fachhochschule Aachen-Jülich, D-52428 Jülich, Germany

Supporting Information

ABSTRACT: 4-Hydroxyphenylacetate decarboxylase is a [4Fe−4S] cluster containing glycyl radical enzyme proposed to use a glycyl/thiyl radical dyad to catalyze the last step of tyrosine fermentation in clostridia. The decarboxylation product *p*-cresol (4-methylphenol) is a virulence factor of the human pathogen *Clostridium difficile*. Here we describe the crystal structures at 1.75 and 1.81 Å resolution of substrate-free and substrate-bound 4-hydroxyphenylacetate decarboxylase from the related *Clostridium scatologenes*. The structures show a $(\beta\gamma)_4$ tetramer of heterodimers composed of a catalytic β-subunit harboring the putative glycyl/thiyl dyad and a distinct small γ-subunit with two [4Fe−4S] clusters at 40 Å distance from the active site. The γ-subunit comprises two domains displaying pseudo-2-fold symmetry that are structurally related to the [4Fe−4S] cluster-binding scaffold of high-potential iron−sulfur proteins. The N-terminal domain coordinates one cluster with one histidine and three cysteines, and the C-terminal domain coordinates the second cluster with four cysteines. Whereas the C-terminal cluster is buried in the $\beta\gamma$ heterodimer interface, the N-terminal cluster is not part of the interface. The previously postulated decarboxylation mechanism required the substrate's hydroxyl group in the vicinity of the active cysteine residue. In contrast to expectation, the substrate-bound state shows a direct interaction between the substrate's carboxyl group and the active site Cys503, while His536 and Glu637 at the opposite side of the active site pocket anchor the hydroxyl group. This state captures a possible catalytically competent complex and suggests a Kolbe-type decarboxylation for *p*-cresol formation.

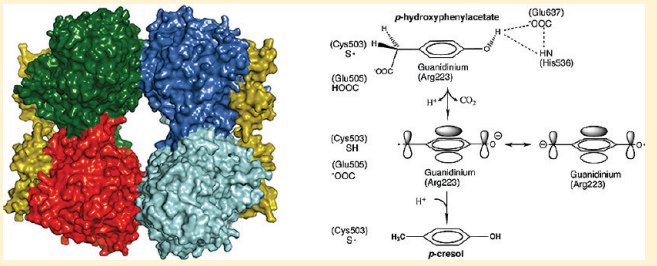

INTRODUCTION

Radical-mediated enzymatic catalysis uses the high reactivity of protein- and/or substrate-based radicals to promote the biological transformation of unreactive compounds in the biosphere. Glycyl radical enzymes (GREs) catalyze chemically challenging reactions in anoxic biological processes such as DNA synthesis (class III ribonucleotide reductase, E.C. 1.17.4.2) and fermentation of glucose (pyruvate formate-lyase, E.C. 2.3.1.54).[1] Functional GREs are generated by post-translational activation by a specific activating enzyme (AE) belonging to the *S*-adenosylmethionine (SAM or AdoMet)-dependent radical superfamily.[2,3] The reductive cleavage of SAM at the SAM-binding [4Fe−4S] cluster of AEs produces methionine and a transient 5′-deoxyadenosyl radical that stereospecifically abstracts a hydrogen atom from a glycine residue in the C-terminus part of the cognate GRE, generating a glycyl radical (storage site).[4] A possible alternative sequence following SAM cleavage has been recently proposed for AE of glycerol dehydratase.[5] It is postulated that substrate binding induces transfer of the radical to the neighboring active site cysteine and hence to the substrate.[6−12] Recently characterized GRE systems acting on aromatic compounds are structurally more complex and contain extra subunits harboring Fe/S clusters.[13] Furthermore, the cognate AEs contain extra Fe/S clusters in addition to the conserved SAM-binding [4Fe−4S] cluster.[13] Examples are benzylsuccinate synthase (E.C. 4.1.99.11) involved in toluene degradation[14,15] and 4-hydroxyphenylacetate decarboxylase (E.C. 4.1.1.83), which catalyzes the last reaction in the fermentative production of *p*-cresol from tyrosine.[16,17] *p*-Cresol is a bacteriostatic substance, and its secretion may benefit the pathogen *Clostridium difficile* by suppression of the endogenous gastrointestinal microflora, allowing the development of gastrointestinal infections.[18,19]

4-Hydroxyphenylacetate decarboxylase is a functional $(\beta\gamma)_4$ heterotetramer (~440 kDa) composed of a 100 kDa catalytic β-subunit harboring the putative glycyl/thiyl active dyad and a small

Received: April 12, 2011
Published: August 08, 2011

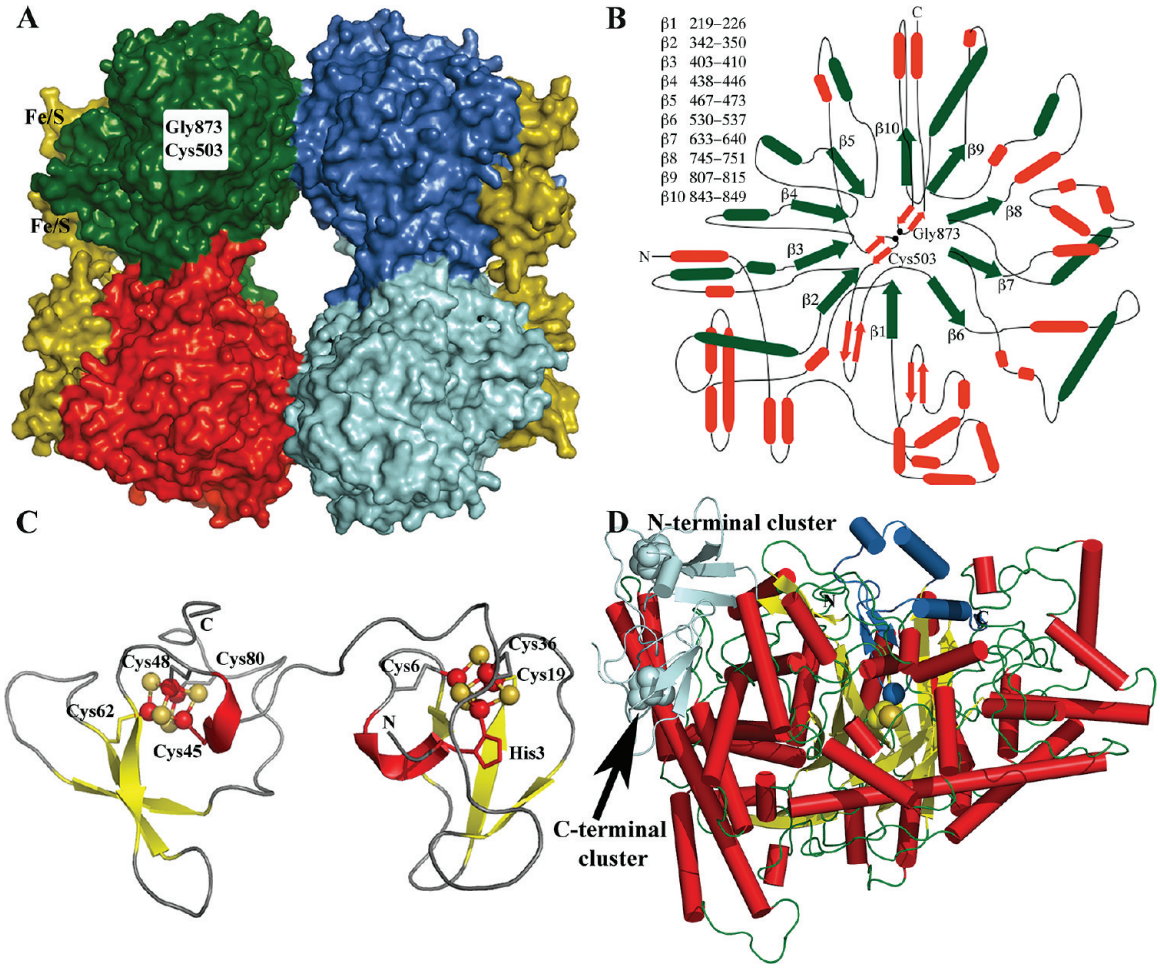

Figure 1. Quaternary structure of 4-hydroxyphenylacetate decarboxylase from *C. scatalogenes*. (A) Molecular surface with β-subunits in green, blue, cyan, and red and γ-subunits in olive. The Fe/S clusters are 20 Å apart and 40 Å from the Cys503/Gly873 dyad. (B) Plumbing diagram of the β-subunit with a canonical GRE fold in green and additional structure elements in orange. (C) Topology of the γ-subunit. The pseudo-2-fold symmetry axis between the two domains (Met1−Ala42 and Glu43−Glu86 for N- and C-terminal domains) runs vertically within the picture plane. (D) β-subunit with radical domain (Asp850−Lys897) in blue and the Cys503/Gly873 dyad in yellow and blue spheres. Gly873 is buried in the barrel core 16 Å below the molecular surface. The γ-subunit (cyan) is shown for easier visualization of its position relative to Cys503/Gly873. The $\beta\gamma$ interface directly includes the C-terminal cluster (labeled C) but not the N-terminal cluster (labeled N).

9.5 kDa γ-subunit that binds two [4Fe−4S] clusters (this work and ref 12). The γ-subunit is proposed to be involved in the regulation of the oligomeric state and catalytic activity of the enzyme.[12] The cognate AE is a 35 kDa monomer with up to two [4Fe−4S] clusters in addition to the SAM-binding [4Fe−4S] cluster.[12] These structural features classify 4-hydroxyphenylacetate decarboxylase in a new subclass of Fe/S cluster containing GREs that also includes benzylsuccinate synthase.[13] The decarboxylation of 4-hydroxyphenylacetate to *p*-cresol is chemically difficult, and the reaction was postulated to involve an Umpolung (polarity inversion)[20] of the aromatic ring and radical intermediates mediated by a one-electron oxidation with either flavin or an Fe/S cluster.[21] Selmer and Andrei characterized the decarboxylase as a GRE and, in analogy to the postulated GRE mechanism,[6−11] proposed the abstraction of the phenolic hydrogen atom by the thiyl radical as the initial catalytic step.[22,23] Observation that 4-hydroxyphenylacetate decarboxylase from *Clostridium scatologenes* (4-HPAD$_{Cs}$) can also convert 3,4-dihydroxyphenylacetate into *p*-methylcatechol and 4-hydroxymandelate (racemic mixture) into *p*-hydroxybenzyl alcohol and the function of 4-hydroxyphenylacetamide as a competitive inhibitor further supported the essential requirement of this functional group.[22]

To access how 4-hydroxyphenylacetate decarboxylase acts at a molecular level, we analyzed the crystal structure of the enzyme from *C. scatologenes* in both substrate-free and substrate-bound (obtained by crystal soaking) states. The observed substrate-binding mode was unexpected but implies a Kolbe-type decarboxylation[24,25] to convert 4-hydroxyphenylacetate into *p*-cresol (Figures 3 and 4). Additionally, we discuss the protein environment of the [4Fe−4S] clusters. We expect our results to help in the design of future experiments to better understand the molecular mechanisms used by Fe/S cluster containing GREs to modulate the radical species' reactivity, which is a fundamental but still poorly understood chemical problem in radical-mediated biocatalysis.

RESULTS AND DISCUSSION

Crystal Structure and Subunit Topology. The crystal structure of 4-HPAD$_{Cs}$ provides the first structural information on an Fe/S cluster containing GRE. The asymmetric unit contains two

dx.doi.org/10.1021/ja203344x |*J. Am. Chem. Soc.* 2011, 133, 14666–14674

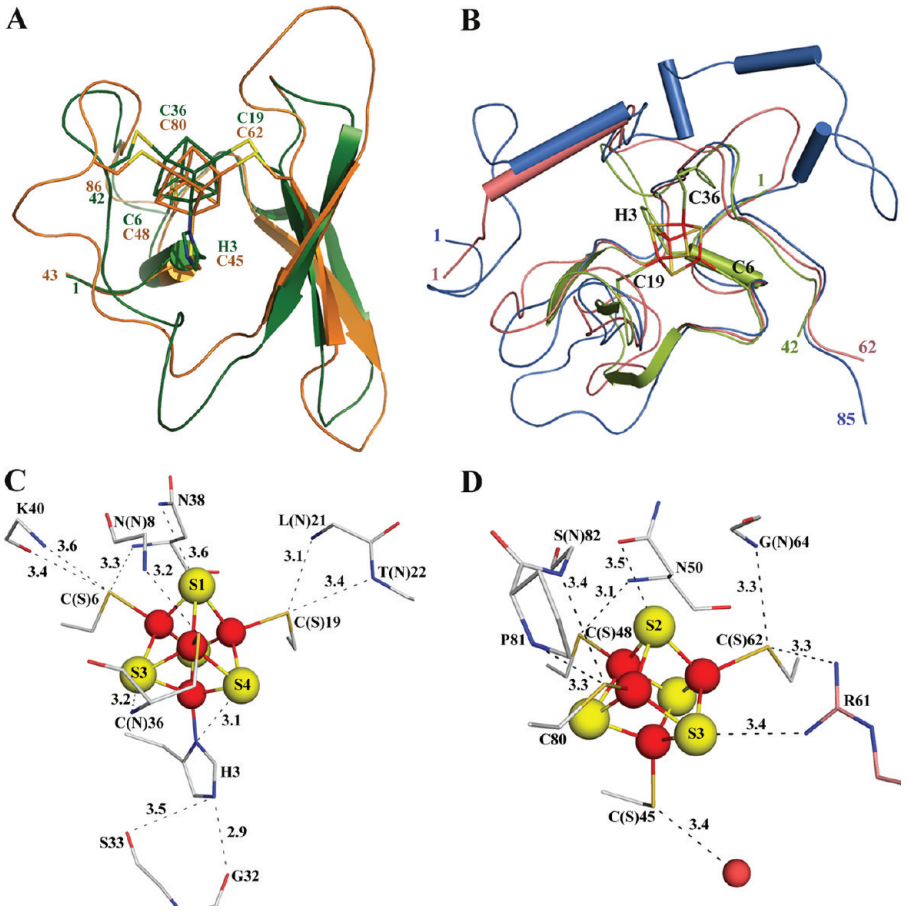

Figure 2. γ-Subunit. (A) Superposition of N- and C-terminal domains (green and orange). (B) N-terminal domain (Met1−Ala42, green) superimposed with two HiPIPs: 1cku (Gln41−Gly85, blue) and 1isu (Lys20−Lys62, salmon). The HiPIPs Fe/S clusters are omitted for clarity. (C, D) Protein environment around the N- and C-terminal clusters with residues at hydrogen-bonding interaction distances (Å) labeled. The average distance value for the possible hydrogen bonds involving the C-terminal cluster is 3.5 Å, indicating weak interactions. Arg61 belongs to the β-subunit.

heterodimers, each comprising one β-subunit and one γ-subunit, and the crystal packing displays a cloverleaf-shaped $(\beta\gamma)_4$ tetramer of heterodimers with $D2$ symmetry (dimensions of $125 \times 95 \times 76$ Å^3 and surface area of roughly 110.000 Å^2) (detailed discussion in Text S1, Supporting Information). The $(\beta\gamma)_4$ heterotetramer is stabilized at two molecular interfaces involving only β-subunits (Figure 1A). Each $\beta\gamma$ heterodimer comprises one catalytic β-subunit containing the Cys503/Gly873 active dyad (Figure 1B,D) and one γ-subunit with two [4Fe−4S] clusters (Figure 1C). The C-terminal [4Fe−4S] cluster and two of its coordinating cysteines are involved in the $\beta\gamma$ heterodimer interface (Figure S1, S9, Supporting Information).

The *catalytic β-subunit* displays the GRE canonical topology: a ten-stranded α/β-barrel composed of two antiparallel five-stranded sheets surrounded by α-helices (Figure 1B).[13] This fold is also present in class I ribonucleotide reductase protein R1,[26] which does not belong to the GRE family. The wide α/β-barrel (inner diameter of ~19 Å between Cα atoms) forms a stable scaffold anchoring two β-hairpin loops opposite one another (Figure 1B,D). One loop extends from the bottom of the barrel and contains Cys503 within a sequence motif characteristic for each GRE (RA[WF][CA]LGGCLE[ST][AS]P for 4-HPAD). The second loop protrudes from the top of the barrel and harbors the radical storage Gly873 within the sequence motif (VRVAGFTQ) that slightly differs from the conserved signature ([STIV]XR[IVT][CSA]GY{GI}[GACV]; http://expasy.org/prosite/PDOC00665). This loop together with two neighboring parallel helices constitutes the C-terminal domain (radical domain, Asp850−Lys897)[27] (Figure 1D). The radical domain is structurally conserved in pyruvate formate-lyase,[28] glycerol dehydratase,[29] and pyruvate formate-lyase 2[30] but not in class III ribonucleotide reductase.[31] 4-HPAD$_{Cs}$ has structural features in addition to the GRE ten-stranded α/β-barrel (Figure S2, Supporting Information). First experimental evidence for a conformational change of the radical domain to position the Gly873-containing loop near the SAM-binding cluster of the cognate AE has been delivered by the crystal structure of pyruvate formate-lyase activating enzyme[27] and biochemical studies on pyruvate formate-lyase.[32] In 4-HPAD$_{Cs}$, two peptide sequences (Gln121−Lys167 and Asn672−Glu700) surrounding the radical domain (Asp850−Lys897) are weakly structured as indicated by an ill-defined electron density (Figure S3, Supporting Information). The peptide regions have no contacts with symmetry-related molecules in the crystal packing. We hypothesize this structural flexibility may contribute to facilitation of the postulated opening of the radical domain upon complex formation with the activating enzyme.[27,29,32]

The *γ-subunit* comprises two domains with 28% amino acid sequence identity that are structurally related by a pseudo-2-fold symmetry indicating a gene duplication origin. The fold of each

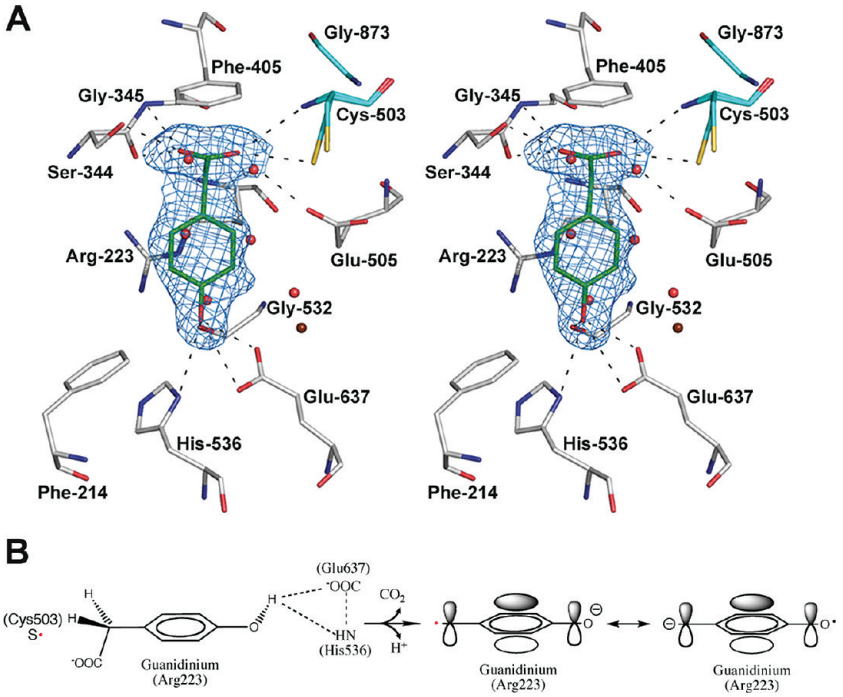

Figure 3. Stereo view of 4-hydroxyphenylacetate bound in the active site. (A) The substrate was omitted for the calculation of the $F_{obs} - F_{calc}$ omit map (blue mesh contoured at 0.35 e/Å^3). The electron density of the omit map for chain C is not so well defined due to a possible second conformation locating the carboxyl group nearer to Cys503 and Glu505. Residues Ile219, Val399, Leu400, Phe537, Val752, and Ile750 were omitted for clarity. Solvent molecules are shown as red spheres (substrate-free state) and a brown sphere (remaining water in the substrate-bound state). Dashed lines indicate interactions at hydrogen-bonding distances (3.4 Å cutoff). (B) Electrostatic configuration of bound 4-hydroxyphenylacetate and possible transition-state radical anion. Estimated distances: 2.5−3 Å between Cys503-Sγ and a possible carboxylic acid hydrogen (RCOOH); 3.5 Å between Cys503-Sγ and the benzylic *Re*-hydrogen (facing Cys503 and Glu505); the benzylic *Si*-hydrogen is more than 5 Å away. See the text for details.

domain contains a helical turn (3_{10}-helix) perpendicular to three antiparallel β-strands (Figure 1C). Superimposition of both domains gives an rms deviation of 1.9 Å for all Cα atoms. The N-terminal domain (green, Figure 2A) binds one [4Fe−4S] cluster through His3, Cys6, Cys19, and Cys36, and the C-terminal domain (orange, Figure 2A) coordinates the second [4Fe−4S] cluster with Cys45, Cys48, Cys62, and Cys80. Whereas both cluster-binding motifs $HX_2CX_{12}CX_{16}C$ and $CX_2CX_{13}CX_{17}C$ are present in the homologous sequence from *C. difficile* ($HX_2CX_{12}CX_{13}C$ and $CX_2CX_{13}CX_{17}C$; UniProt accession code Q84F15), only the C-terminal cluster-binding motif is present in the sequence from *Tannerella forsythensis* ATCC 43037 ($CX_2CX_{14}CX_{16}C$; gene ID TF1151). A similar 4-cysteine sequence motif is present in the β- and γ-subunits of benzylsuccinate synthase from *Thauera aromatica* ($CX_2CX_{14-19}CX_{22}C$; UniProt accession codes O87944 and O87942, respectively) and *Azoarcus* sp. T ($CX_2CX_{14-19}CX_{22-23}C$; UniProt accession codes AAK50373 and Q8VPT8, respectively). The γ-subunit of 4-HPAD$_{Cs}$ has no sequence similarity to any protein with known function, but the two domains are structurally similar to high-potential iron−sulfur proteins (HiPIPs). HiPIPs have an N-terminal extension of 20−40 residues, so the structural similarity is limited to their Fe/S cluster-binding scaffold (Figure 2B). Superposition of both γ-subunit domains with this scaffold gives rms deviation values for all Cα atoms of 1.4 and 1.9 Å for N- and C-terminal domains with PDB ID code 1cku,[33] and 1.3 and 1.7 Å for N- and C-terminal domains with PDB ID code 1isu.[34] Albeit the weak amino acid sequence identity (13% with 1cku and 18% with 1isu), the cluster binding motifs are remarkably similar to $H/CX_2CX_{12-13}CX_{16-17}C$ for the γ-subunit and $CX_2CX_{13-19}CX_{14-19}C$ for HiPIPs. Hence, we propose the two domains from the γ-subunit are most probably derived from a duplication of the HiPIPs cluster-binding scaffold region.

Active Site Topology and Substrate Binding. The active site pocket of 4-HPAD$_{Cs}$ has dimensions of 14 × 12 × 10 Å^3 (interatomic distances between Cβ atoms of Arg223 and Val752, Ser344 and Ile750, and Cys503 and His536) and is embedded in the core of the ten-stranded α/β-barrel (Figure 1D). It is accessed by a funnel-shaped crevice that spans 24 Å from the molecular surface to Cys503 that likely harbors a thiyl radical during catalysis (a variant enzyme with Cys503 mutated to Ser is inactive) (Figure S4A, S4B, Supporting Information).[35] The putative radical storage site Gly873 is at a 4.7 Å distance from Cys503 and is not part of the active site pocket (Figure S4B, S4C, Supporting Information). In the substrate-free state, the void volume of the pocket is filled with six water molecules at hydrogen-bonding interaction distances (3.4 Å distance cutoff, Figure S4C, Supporting Information). Two waters are bridged between Ser344 and Cys503 with a short interatomic distance (2.5 Å), and one water molecule is at hydrogen-bonding interaction distance from Glu637. Solvent molecules are displaced upon substrate binding, and the location of five waters is taken over by atoms of the substrate: the carboxyl group substitutes the two waters bridging Ser344 to Cys503, the aromatic ring expels two additional waters, and the hydroxyl group replaces the water adjacent to Glu637 (Figure 3A). Thus, 4-hydroxyphenylacetate is neatly bound in the active site through an extensive network of hydrogen-bonding interactions involving the carboxyl group with Ser344, Gly345, Cys503, and

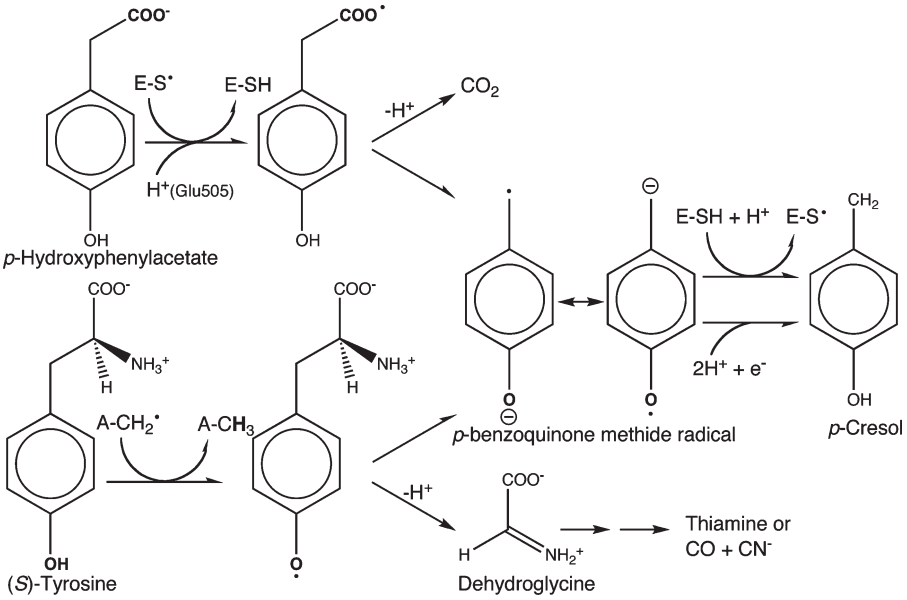

Figure 4. Proposed mechanism for the GRE 4-hydroxyphenylacetate decarboxylases (upper reactions) and the SAM radical enzymes tyrosine lyases (lower reactions). Both enzymes are proposed to catalyze the formation of the same *p*-benzoquinone methide radical anion intermediate, but the pathways are different. E−S· = thiyl of cysteine 503 in 4-HPAD; A-CH3 = 5′-deoxyadenosine. The nature of the final electron donor for tyrosine lyase has not been established.

Glu505 and the hydroxyl group with His536 and Glu637. The substrate's conformation is further constrained by a π-cation interaction between the aromatic ring's face and Nε2 of Arg223 and by van der Waals interactions with the side chains of Phe214, Ile219, Arg223, Val399, Leu400, Phe405, Phe537, Ile750, and Val752. Additionally, the hydroxyl group is at distances of 3.4 and 3.6 Å from the aromatic ring edges of Phe214 and Phe537, respectively, and the parallel orientation of the carboxymethyl moiety with the aromatic ring face of Phe405 places both carboxyl oxygen atoms ca. 3.5 Å from the ring edge of Phe405. The carboxymethyl moiety is almost perpendicular to the phenyl moiety, displaying a conformation required for decarboxylation: near-parallel alignment of the orbitals of the C−C bond between the carboxyl and the methylene group with the p-orbitals of the ring π-system (Figure 3B). Furthermore, the hydrogen bond interaction between the hydroxyl group and Glu637/His536 further constrains the electronic configuration by aligning a lone pair orbital of the phenolic oxygen atom with the π-orbitals of the phenyl ring (Figure 3B).

Substrate binding induces a movement of the Gly873 loop toward Cys503 by 0.4 Å to 4.3 Å from its position in the substrate-free state. With the exception of Cys503, Leu504, and Glu505, all side chains at or near the active site pocket display the same conformation as in the substrate-free state (Figure S5, Supporting Information). We observe an additional conformation for Cys503 that differs slightly between the two independent molecules in the asymmetric unit (Table S2, Supporting Information). The side chain of Leu504 rotates by 90°, and the electron density map indicates a possible movement of Glu505 toward the substrate's carboxyl group. The observed flexibility of the Gly873 and Cys503 loops gives insight into how substrate binding may promote the conformational rearrangement of the loops to generate the thiyl radical and then to transfer the radical to the substrate to start the reaction. In the structurally characterized GREs (Figure S6, Supporting Information), the Gly$C\alpha$−Cys$S\gamma$ interatomic distance ranges from 3.5 Å for pyruvate formate-lyase (pyruvate-bound state; PDB ID code 1h16) to 5.2 Å for class III ribonucleotide reductase (Gly580 substituted by Ala; PDB ID code 1hk8). For glycerol dehydratase, the interatomic distance decreases from 4.4 Å in the substrate-free state to 4.0 Å in the glycerol-bound state (PDB ID code 1r9d). Similar distances (3.5−4.1 Å) for direct hydrogen atom abstraction were reported for the SAM radical enzymes coproporphyrinogen-III oxidase (distance postulated from modeled substrate),[36] biotin synthase,[37] lysine-2,3-aminomutase,[38] and pyruvate formate-lyase activating enzyme.[27] The active site pockets of structurally characterized GREs are, with the exception of class III ribonucleotide reductase, hydrophobic and upon substrate binding become compact with tight van der Waals contacts. The active site of 4-HPAD$_{Cs}$ is most similar to that of glycerol dehydratase, with the carboxyl group of 4-hydroxyphenylacetate superimposing with the C2−C3(OH) moiety of glycerol (Figure S7A, Supporting Information). Comparison with pyruvate formate-lyase 2 superimposes the carboxyl group of 4-hydroxyphenylacetate with the C1−C2(OH) moiety of glycerol (Figure S7B, Supporting Information), and comparison with pyruvate formate-lyase superimposes the carboxyl group of 4-hydroxyphenylacetate with Cys418 (Figure S7C, Supporting Information). As for class I ribonucleotide reductase protein R1, the carboxymethyl moiety of 4-hydroxyphenylacetate superimposes with the ribose ring of guanosine diphosphate, with one carboxyl oxygen occupying a position similar to that of the C2′−OH group of guanosine diphosphate (Figure S7D, Supporting Information). The structural comparison of substrate-free and substrate-bound states suggests the active site of 4-HPAD$_{Cs}$, like that first observed for pyruvate formate-lyase,[28] has a ready-to-bind architecture allowing substrate binding without substantial structural rearrangements.

Possible Mechanism of 4-Hydroxyphenylacetate Decarboxylation. Before the structure was solved, a mechanism for decarboxylation of 4-HPA was deduced on the basis of theoretical considerations, which starts with the abstraction of a

hydrogen from the phenolic hydroxyl group of the substrate.[21,22] The postulated mechanism required the substrate's hydroxyl group in the vicinity of the active cysteine residue,[22] which we do not observe in the structure.

The crystal structure offers an unexpected substrate-binding mode for 4-hydroxyphenylacetate with its carboxyl group in the direct vicinity of Cys503 (Figure 3A) and thus provides experimental support to formulate a Kolbe-type decarboxylation mechanism. Kolbe electrolysis is defined as the one-electron oxidation of carboxylate ions (RCO_2^-), generating alkyl radicals after decarboxylation.[24,25] A one-electron oxidation mediated decarboxylation of carboxylic acids possessing aromatic substituent(s) at the α-position has been described for a cytochrome P450 system.[39] The resulting carboxyl radical ($R-COO^\bullet$) readily decomposes to afford carbon dioxide and an alkyl radical, where the rate of decarboxylation (k_{dec}) of $R-COO^\bullet$ is strongly modulated by the structure of the R moiety, with k_{dec} of $C_6H_5-CH_2-COO^\bullet$ about 50 times larger than k_{dec} of $C_6H_5-COO^\bullet$.[39,40] The redox potential values (E_m vs NHE at pH 7) of 1.33 V for $(CysS^\bullet + H^+ + e^-)/CysSH$[41] and 1.40 V for $(R^\bullet + CO_2 + e^-)/R-COO^-$ (R = C_6H_5; no available data for $HO-C_6H_4-CH_2$)[42] make it thermodynamically feasible that, in the first step of the decarboxylation reaction, the thiyl radical Cys503-S$^\bullet$ could oxidize the substrate's carboxylate anion to a radical (Figure 4). Since according to continuum electrostatic calculations Glu505 and the substrate share a proton, the generated thiolate could be protonated by this residue (at a 3 Å distance). This unusual titration behavior is caused by the structural proximity of the carboxyl group of Glu505 to the substrate's carboxyl group and is not unusual for clusters of charged residues.[43,44] Hence, the electron transfer from the carboxylate to Cys503-S$^\bullet$ and the protonation of the resulting thiolate could be coupled. According to a concerted decarboxylation mechanism, the transfer of the radical from Cys503 to the substrate would generate the radical $HO-C_6H_4-CH_2^\bullet$ and CO_2. The removal of the phenolic proton by Glu637 and a π-cation interaction with the guanidinium moiety of Arg223 may further contribute to the resonance stabilization of the ketyl-like *p*-benzoquinone methide radical anion ($^-O-C_6H_4-CH_2^\bullet \leftrightarrow {}^\bullet O-C_6H_4-CH_2^-$) (Figures 3B and 4).[21,22] The same radical anion has been proposed to participate in the reaction of anaerobic SAM-dependent tyrosine lyase that catalyzes the formation of dehydroglycine for the synthesis of the thiazole ring of thiamine diphosphate (Figure 4).[45] A similar enzyme is also involved in the formation of cyanide and CO for the active site of [FeFe]hydrogenase.[46] In contrast to *p*-hydroxyphenylacetate, the fragmentation of tyrosine to dehydroglycine and the *p*-benzoquinone methide radical anion can only proceed by abstracting the phenolic hydrogen by the 5′-deoxyadenosyl radical derived from SAM, as proposed earlier for the mechanism of 4-HPAD.[21,22] This hydrogen abstraction is thermodynamically favored by 50 kJ/mol.[47] The stability of the *p*-benzoquinone methide radical anion is probably the reason why nature chose tyrosine as the precursor of dehydroglycine. Thus, *p*-hydroxyphenylacetate and tyrosine generate the same radical intermediate by selecting the thermodynamically most feasible mechanism for each substrate (Figure 4). 4-HPAD$_{Cs}$ probably quenches this *p*-benzoquinone methide radical anion by hydrogen atom or proton-coupled electron transfer from Cys503 and protonation by Glu637 to yield *p*-cresol and regenerate the thiyl radical. The byproduct CO_2 can diffuse through the protein matrix. Thus, the essential OH group in the *para*-position could have two functions. It anchors the substrate in the active site by hydrogen bonds to His536 and Glu637 and after deprotonation favors the formation of the stabilized *p*-benzoquinone methide radical anion.

Manual modeling based on the substrate-binding mode locates the additional hydroxyl group of 3,4-dihydroxyphenylacetate in a cavity between Glu505 and Glu637 with likely hydrogen-bonding interactions with Glu637. A solvent molecule occupies this cavity in both the substrate-bound and substrate-free states (brown sphere in Figure 3A). Superposition of 4-hydroxymandelate suggests the hydroxyl group of one enantiomer can dock at a cavity formed by the side chains of Leu400, Phe405, Cys503, and Val752. The competitive inhibitor 4-hydroxyphenylacetamide contains the hydroxyl group needed for correct orientation within the active site pocket, but in contrast to the acetate moiety in the physiologic substrate, the acetamide moiety cannot be decarboxylated.[22] To our knowledge, 4-hydroxyphenylacetate decarboxylase is the first characterized radical-dependent enzyme using a Kolbe mechanism.

Protein Environment of the [4Fe−4S] Clusters. As-isolated, 4-HPAD$_{Cd}$ and 4-HPAD$_{Cs}$ show spectroscopic features for partially reduced clusters ($[4Fe-4S]^{1+}$), and a single reduction potential of −287 mV ± 4 mV (vs NHE) was determined for 4-HPAD$_{Cd}$, indicating that only one of the clusters is redox active.[35,48] The value observed for 4-HPAD$_{Cd}$ and postulated for 4-HPAD$_{Cs}$ is within the range observed for the reduction of ferredoxins ($[4Fe-4S]^{2+}$ to $[4Fe-4S]^{1+}$ couple) with associated reduction potential between −250 and −400 mV (vs NHE).[49] Thus, the Fe−S clusters present in the γ-subunit have a binding motif similar to that of HiPIPs, but the detected redox active cluster is able to cycle between the 2+/1+ couple like ferredoxins. Whereas ferredoxins cycle between the 2+/1+ states at negative reduction potentials, the HiPIPs function at positive reduction potentials (+90 to +460 mV (vs NHE) for the 3+/2+ couple).[50,51] The protein environment modulates the redox potential of Fe/S clusters, and contributing factors are hydrogen-bonding networks (especially NH---S bonds), peptide dipoles, and specific charged residues surrounding the cluster, as well as solvent exposure of the cluster.[52−54,49] The solvent accessibility of the cluster seems to account for most of the difference between ferredoxin and HiPIP reduction potentials.[55,49] The smaller number of hydrogen bonds (five conserved interactions)[52] and the hydrophobic environment[56] also contribute to stabilization of the lower net charge on the HiPIP cluster (3+ state) relative to ferredoxins, which have a solvent-accessible cluster with a larger number of hydrogen bonds.[55,57]

The N-terminal cluster is solvent shielded, and the majority of the hydrogen bond interactions are between sulfide/thiolates and the peptide backbone (Figure 2C). There are three additional interactions with the conserved HiPIP hydrogen-bonding network (Figure S8A, S8B and Table S3, Supporting Information). Hydrogen bonding to the Fe−S cluster ligands reduces their charge donation to the Fe ions, decreasing the Fe−S bond covalency and increasing the effective nuclear charge of the Fe ions. Thus, it becomes easier to reduce the cluster, and the respective reduction potential value increases.[55,58] Histidine as a neutral ligand (His3(Nδ1)-bound Fe) could help to stabilize a reduced state of the cluster ($[4Fe-4S]^{1+}$). Similarly, the larger number of hydrogen bonds in ferredoxin (eight conserved interactions) stabilizes the negatively charged reduced 1+ state relative to HiPIP.[52] The N-terminal cluster environment displays

common residues relative to HiPIPs (Figure S8C, Supporting Information). In HiPIPs, the hydrophobic environment promotes the oxidized electronic 3+ state because of the few or nonpolar residues in the vicinity of the cluster that could dissipate the higher net charges on the cluster.[55,59] The additional polar residues in the vicinity of the N-terminal cluster may help dissipate a higher net charge of a reduced cluster ($[4Fe-4S]^{1+}$). As expected from a gene duplication origin, the residues in the vicinity of the C-terminal cluster are similar to the ones surrounding the N-terminal cluster, but the environment is less hydrophobic (Figures S8D and Supporting Information). In contrast to the N-terminal cluster, the C-terminal cluster displays few and weaker NH/OH---S interactions involving only two sulfide ligands (Figure 2D; Table S3, Supporting Information). Structurally, the C-terminal cluster and two of its coordinating cysteines (Cys62 and Cys80) are part of the $\beta\gamma$ heterodimer interface and interact with secondary structure elements of the β-subunit involved in the β/β interface within the $(\beta\gamma)_4$ heterotetramer (Met53−Glu65 and Asn284−Ile301, Figures S1, S2, and S9, Supporting Information). Without the contacts made with the β-subunit, the C-terminal cluster would be highly solvent accessible (sulfide ligands S2 and S3 and the two Cys62 and Cys80 located at the molecular surface).

In conclusion, the N-terminal cluster displays a higher number of hydrogen bonds relative to HiPIPs, but its environment is quite similar with only one extra polar residue. Moreover, the cluster is not as deeply buried as observed in HiPIPs (4.5 Å below the surface)[56] with the sulfide ligand S4 at the molecular surface. The C-terminal cluster displays a lower number of hydrogen bonds relative to the N-terminal cluster but still higher than for HiPIPs, its cluster environment is less hydrophobic (two extra polar residues and a solvent molecule), and the cluster is completely protected from direct solvent contact by the β-subunit. The [4Fe−4S] cluster present in the γ-subunit of benzylsuccinate synthase also appears to be necessary for structural integrity, whereas the function of the second small β-subunit and its cluster is still not clear.[15]

Functional Modifications of 4-HPAD$_{Cs}$. Upon activation, 4-HPAD$_{Cs}$ reaches maximum specific activity within 10 min, after which the radical decays with a half-life of about 40 min. This decay is only observed in the absence of substrate and is accompanied by a [4Fe−4S] cluster oxidation.[12,48] Apparently, an electron is transferred from one of the two clusters to the Gly873 radical that was converted to a carbanion followed by protonation. This process makes 4-HPAD$_{Cs}$ unique among GREs that otherwise display a slow activation and a stable glycyl radical during prolonged anaerobic incubation.[8,60] The shortest distance between the two clusters of 4-HPAD$_{Cs}$ and Gly873 is around 40 Å. In class I ribonucleotide reductase, the mechanism of thiyl radical formation was proposed to involve a long-range proton-coupled electron transfer from the binuclear Fe site over a 35 Å distance[26,61] requiring the involvement of transient aromatic amino acid radical intermediates.[62,63] Experimental evidence is accumulating for the feasibility and physiological relevance of such long-range electron transfer processes in other radical-dependent enzyme systems.[64,65]

CONCLUSIONS

Our structural analysis of 4-HPAD$_{Cs}$ in the substrate-free and substrate-bound states together with biochemical studies[12,22] revealed the oligomeric state of the catalytically competent enzyme and the stoichiometry of the additional [4Fe−4S] clusters and enabled us to postulate a Kolbe-type decarboxylation mechanism for substrate conversion. We also gained insight into putative structural rearrangements for radical transfer from the activating enzyme to the storage Gly873 and hence to the catalytic Cys503 and possible redox properties of the two [4Fe−4S] clusters present in the γ-subunit. 4-Hydroxyphenylacetate decarboxylase is the prototype of a more complex GRE subclass in which the typical HiPIP cluster-binding scaffold was duplicated and specifically modified to create the γ-subunit. The additional Fe/S cluster containing subunit(s) present in 4-HPAD and benzylsuccinate synthase most probably represent a gain of function for this novel Fe/S cluster containing GRE subclass, and in the case of 4-HPAD the host organisms evolved regulatory mechanisms for an efficient response to environmental changes to achieve maximal ability to thrive. Future experiments are necessary to clarify and better understand the role(s) of the Fe/S cluster in catalysis.

EXPERIMENTAL SECTION

Anoxic Crystallization and Data Collection. Recombinant 4-HPAD$_{Cs}$ was crystallized in an anoxic glovebox (95% N_2, 5% H_2 atmosphere, Coy, United States). Crystals were obtained by the hanging-drop vapor diffusion method by mixing 1:1 protein (40 mg mL^{-1}) with precipitant (22% PEG MME 550, 30 mM $MgCl_2$, 100 mM Tris/HCl pH 7.5−8.4). Substrate-bound crystals were obtained by soaking crystals in precipitant containing 20−50 mM 4-hydroxyphenylacetate. The crystals have space group $C222(1)$ and cell constants of a = 132.28 Å, b = 227.75 Å, and c = 148.01 Å, corresponding to two heterodimers per asymmetric unit and a solvent content of 54%. Crystals were harvested in precipitant and shock-frozen, and diffraction data were collected at 100 K on a rotating Cu anode X-ray generator (Nonius FR591, Bruker AXS, Germany) coupled to an image plate (mar345dtb, Marresearch, Germany). Diffraction data were processed and scaled with XDS.[66]

Structure Determination and Refinement. The crystal structure was determined by phase combination. The phases obtained by Patterson search techniques[67] with an edited model of glycerol dehydratase were used to locate four [4Fe−4S] clusters in anomalous difference Fourier maps. Individual Fe positions were used for SAD phasing with SHARP.[68] Automatic model building with ARP/warp[69] resulted in a largely complete polypeptide. Model building was done with COOT[70] and initial positional and temperature refinement with CNS.[71] A final refinement cycle was performed with Phenix[72] using TLS-refinement for the substrate-bound state. The refined model of substrate-free 4-HPAD$_{Cs}$ contains two β-subunits (Asp29−Lys897), two γ-subunits (Met1−Glu86), four [4Fe−4S] clusters, and 2145 water molecules. The refined model of the substrate-bound complex displays the same polypeptide and [4Fe−4S] cluster composition, one substrate molecule per active site, and 2147 solvent molecules. The b-factors for the substrate are in the same value range as for the surrounding residues. The N-terminal residues Met1−Ala28 from both β-subunits were not visible in the electron density map and therefore not incorporated into the refined models. The polypeptide regions Phe689−Lys695 and Pro687−Lys695 of the two β-subunits, located at the surface of the molecule, were not clearly defined in the electron density map and were modeled with one of the possible conformers. Refinement statistics and stereochemistry analysis done with Molprobity as implemented in Phenix are presented in Table S1 (Supporting Information). The protein model for the substrate-free state displays four outlier residues in the β-subunit: Met98, Pro529, Phe537, and Asp694. With the exception of Asp694 located at the surface, all outliers are well-defined

in the electron density map. For the substrate-bound state, the outlier residues Met98, Pro529, and Phe537 (β-subunit) and Asn53 (γ-subunit) are well-defined in the electron density map. Molecular interfaces were calculated with PISA as implemented in the CCP4 suite[73] and cavities with CASTp.[74] Structure comparisons were calculated with Dali[75] and SSM.[76] Figures were prepared with PyMOL.[77] Distances discussed in the text are the average value between the two independent $\beta\gamma$ heterodimers observed in the asymmetric unit. Atomic coordinates and structure factors have been deposited with the Protein Data Bank (www.pdbe.org) and will be release for publication (PDB ID codes: 2y8n and r2y8nsf for substrate-free, 2yaj and r2yajsf for substrate-bound).

Calculation of Protonation Probabilities. The protonation of all other protonatable residues in the substrate-bound state were calculated using a continuum electrostatic approach combined with a Monte Carlo (MC) titration.[78] The Poisson−Boltzmann equation was solved by a finite-difference method using the MEAD program suite.[79] All aspartate, histidine, glutamate, lysine, arginine, and tyrosine residues as well as the carboxyl group of the ligand were considered as protonatable sites. Atomic partial charges for standard amino acid groups were taken from the CHARMM27 parameter set,[80] and the pK_a values of the model compounds were taken from the literature.[78] The dielectric constant of the protein was set to 4, and that of the solvent was set to 80. The ionic strength was set to 0.1 M. The thickness of the ion exclusion layer was set to 2.0 Å. Protonation probabilities were calculated for pH values of 0−14 in steps of 0.2 using Metropolis MC. The temperature was set to 300 K. At each pH value, a randomly chosen initial state vector was equilibrated with 200 MC scans, where one MC scan comprises as many MC moves as there are titratable sites in the protein. Subsequently, 5000 MC scans were performed to determine the protonation probability of each site of the protein.

■ ASSOCIATED CONTENT

Supporting Information. Crystallographic statistics, tables, text, figures, and complete refs 18, 72, and 80. This material is available free of charge via the Internet at http://pubs.acs.org.

■ AUTHOR INFORMATION

Corresponding Author
berta.martins@biologie.hu-berlin.de

■ ACKNOWLEDGMENT

We are grateful to B. T. Golding (Newcastle University), J. Stubbe (Massachusetts Institute of Technology), and H. Dobbek (Humboldt-Universität zu Berlin) for helpful discussions. We also acknowledge all four reviewers for valuable suggestions. We thank S. Werner (Philipps-Universität Marburg) for technical assistance. This work was supported by the DFG SPP 1319 (B.M. M., M.F., G.M.U., W.B.), DFG SPP 1071 (M.B., T.S., W.B.), Elitenetzwerk Bayern (B.M.M., M.F.), and Fonds der Chemische Industrie (B.M.M., W.B.).

■ REFERENCES

(1) Eklund, H.; Fontecave, M. *Structure* **1999**, *7*, 257–262.
(2) Sofia, H. J.; Chen, G.; Hetzler, B. G.; Reyes-Spindola, J. F.; Miller, N. E. *Nucleic Acids Res.* **2001**, *29*, 1097–106.
(3) Frey, P. A.; Hegeman, A. D.; Ruzicka, F. J. *Crit. Rev. Biochem. Mol. Biol.* **2008**, *43*, 63–88.
(4) Frey, P. A.; Hegerman, A. D.; Reed, G. H. *Chem. Rev.* **2006**, *106*, 3302–3316.
(5) Demick, J. M.; Lanzilotta, W. N. *Biochemistry* **2011**, *50*, 440–442.
(6) Knappe, J.; Neugebauer, F. A.; Blaschkowski, H. P.; Gänzler, M. *Proc. Natl. Acad. Sci. U.S.A.* **1984**, *81*, 13321–1335.
(7) Wagner, A. F.; Frey, M.; Neugebauer, F. A.; Schafer, W.; Knappe, J. *Proc. Natl. Acad. Sci. U.S.A.* **1992**, *89*, 996–1000.
(8) Frey, M.; Rothe, M.; Wagner, A. F. V.; Knappe, J. *J. Biol. Chem.* **1994**, *269*, 12432–12437.
(9) Sun, X.; Ollagnier, S.; Schmidt, P. P.; Atta, M.; Mulliez, E.; Lepape, L.; Eliasson, R.; Graslund, A.; Fontecave, M.; Reichard, P.; Sjoberg, B. M. *J. Biol. Chem.* **1996**, *271*, 6827–6831.
(10) Young, P.; Andersson, J.; Sahlin, M.; Sjoberg, B. M. *J. Biol. Chem.* **1996**, *271*, 20770–20775.
(11) Krieger, C. J.; Roseboom, W.; Albracht, S. P. J.; Spormann, A. M. *J. Biol. Chem.* **2001**, *276*, 12924–12927.
(12) Yu, L.; Blaser, M.; Andrei, P. I.; Pierik, A. J.; Selmer, T. *Biochemistry* **2006**, *45*, 9584–9592.
(13) Selmer, T.; Pierik, A. J.; Heider, J. *Biol. Chem.* **2005**, *386*, 981–988.
(14) Leuthner, B.; Leutwien, C.; Schulz, H.; Horth, P.; Haehnel, W.; Schiltz, E.; Schagger, H.; Heider, J. *Mol. Microbiol.* **1998**, *28*, 615–28.
(15) Li, L.; Patterson, D. P.; Fox, C. C.; Lin, B.; Coshigano, P. W.; Marsh, E. N. G. *Biochemistry* **2009**, *48*, 1284–1292.
(16) D'Ari, L.; Barker, H. A. *Arch. Microbiol.* **1985**, *143*, 311–312.
(17) Andrei, P. I.; Pierik, A. J.; Zauner, S.; Andrei-Selmer, L. C.; Selmer, T. *Eur. J. Biochem.* **2004**, *271*, 2225–2230.
(18) Sebaihia, M.; *et al. Nat. Genet.* **2006**, *38*, *779–786.*
(19) Dawson, L. F.; Stabler, R. A.; Wren, B. W. *J. Med. Microbiol.* **2008**, *57*, 745–749.
(20) Seebach, D. *Angew. Chem., Int. Ed. Engl.* **1979**, *18*, 239–258.
(21) Buckel, W.; Golding, B. T. *FEMS Microbiol. Rev.* **1999**, *22*, 523–41.
(22) Selmer, T.; Andrei, P. I. *Eur. J. Biochem.* **2001**, *268*, 1363–1372.
(23) Buckel, W. *Angew. Chem., Int. Ed.* **2009**, *48*, 6779–6787.
(24) Kolbe, H. *Ann. Chim. Pharm.* **1849**, *69*, 257–294.
(25) Vijh, A. K.; Conway, B. E. *Chem. Rev.* **1967**, *67*, 623–664.
(26) Uhlin, U.; Eklund, H. *Nature* **1994**, *370*, 533–539.
(27) Vey, J. L.; Yang, J.; Li, M.; Broderick, W. E.; Broderick, J. B.; Drennan, C. L. *Proc. Natl. Acad. Sci. U.S.A.* **2008**, *105*, 16137–16141.
(28) Becker, A.; Fritz-Wolf, K.; Kabsch, W.; Knappe, J.; Schultz, S.; Wagner, A. F. V. *Nat. Struct. Biol.* **1999**, *6*, 969–975.
(29) O'Brien, J. R.; Raynaud, C.; Croux, C.; Girbal, L.; Soucaille, P.; Lanzilotta, W. N. *Biochemistry* **2004**, *43*, 4635–4645.
(30) Lehtio, L.; Grossmann, J. G.; Kokona, B.; Fairman, R.; Goldman, A. *J. Mol. Biol.* **2006**, *357*, 221–235.
(31) Logan, D. T.; Mulliez, E.; Larsson., K. M.; Bodevin, S.; Atta, M.; Garnaud, P. E.; Sjoberg, B. M.; Fontecave, M. *Proc. Natl. Acad. Sci. U.S.A.* **2003**, *100*, 3826–3831.
(32) Peng, Y.; Veneziano, S. E.; Gillispie, G. D.; Broderick, J. B. *J. Biol. Chem.* **2010**, *285*, 27224–27231.
(33) Parisini, E.; Capozzi, F.; Lamzin, V.; Luchinat, C.; Sheldrick, G. M. *Acta Crystallogr., Sect. D: Biol. Crystallogr.* **1999**, *55*, 1773–1784.
(34) Rayment, I.; Wesenberg, G.; Meyer, T. C.; Cusanovich, M. A.; Holden, H. M. *J. Mol. Biol.* **1992**, *228*, 672–686.
(35) Yu, L. Two novel glycyl radical decarboxylase systems from *Clostridium scatologenes* and *Tannerella forsythensis*. Ph.D. Thesis, Philipps-Universität Marburg, Marburg, Germany, 2006.
(36) Layer, G.; Moser, J.; Heinz, D. W.; Jahn, D.; Schubert, W. D. *EMBO J.* **2003**, *22*, 6214–624.
(37) Berkovitch, F.; Nicolet, Y.; Wan, J. T.; Jarrett, J. T.; Drennan, C. L. *Science* **2004**, *303*, 76–79.
(38) Lepore, B. W.; Ruzicka, F. J.; Frey, P. A.; Ringe, D. *Proc. Natl. Acad. Sci. U.S.A.* **2005**, *102*, 13819–13824.
(39) Komuro, M.; Higuchi, T.; Hirobe, M. *Bioorg. Med. Chem.* **1995**, *3*, 55–65.
(40) Sasaki, K.; Uneyama, K.; Nagura, S. *Electrochim. Acta* **1966**, *11*, 891–894.
(41) Surdhar, P.; Armstrong, D. A. *J. Phys. Chem.* **1987**, *91*, 6532–6537.
(42) Eberson, L. *Acta Chem. Scand.* **1963**, *17*, 2004–2018.

(43) Klingen, A. R.; Bombarda, E.; Ullmann, G. M. *Photochem. Photobiol. Sci.* **2006**, *5*, 588–596.
(44) Crnogorac, M. M.; Ullmann, G. M.; Kostic, N. M. *J. Am. Chem. Soc.* **2001**, *123*, 10789–10798.
(45) Challand, M. R.; Martins, F. T.; Roach, P. L. *J. Biol. Chem.* **2010**, *285*, 5240–5248.
(46) Driesener, R. C.; Challand, M. R.; McGlynn, S. E.; Shepard, E. M.; Boyd, E. S.; Broderick, J. B.; Peters, J. W.; Roach, P. L. *Angew. Chem., Int. Ed.* **2010**, *49*, 1687–1690.
(47) Hioe, J.; Zipse, H. *Org. Biomol. Chem.* **2010**, *8*, 3609–3617.
(48) Blaser, M. Activation and Regulation of the 4-hydroxyphenylacetate decarboxylase system from *Clostridium difficile*. Ph.D. Thesis, Philipps-Universität Marburg, Marburg, Germany, 2006.
(49) Dey, A.; Jenney, F. E. J.; Adams, M. W. W.; Babini, E.; Takahashi, Y.; Fukuyama, K.; Hodgson, K. O.; Hedman, B.; Solomon, E. I. *Science* **2007**, *318*, 1464–1468.
(50) Meyer, T. E.; Przysiecki, C. T.; Watkins, J. A.; Bhattacharyya, A.; Simondsen, R. P.; Cusanovich, M. A.; Tollin, G. *Proc. Natl. Acad. Sci. U.S.A.* **1983**, *80*, 6740–6744.
(51) Capozzi, F.; Ciurli, S.; Luchinat, C. *Struct. Bonding (Berlin)* **1998**, *90*, 127–160.
(52) Sheridan, R. P.; Allen, L. C.; Carter, C. W. *J. Biol. Chem.* **1981**, *256*, 5052–5057.
(53) Jensen, G. M.; Warshel, A.; Stephens, P. J. *Biochemistry* **1994**, *33*, 10911–10924.
(54) Hunsicker-Wang, L. M.; Heine, A.; Chen, Y.; Luna, E. P.; Tadaro, T.; Zhang, Y. M.; Wiliams, P. A.; McRee, D. E.; Hirst, J.; Stout, C. D.; Fee, J. A. *Biochemistry* **2003**, *42*, 7303–7317.
(55) Backes, G.; Mino, Y.; Loehr, T. M.; Meyer, T. E.; Cusanovich, M. A.; Sweeney, W. V.; Adman, E. T.; Sandersloehr, J. *J. Am. Chem. Soc.* **1991**, *113*, 2055–2064.
(56) Carter, C. W.; Kraut, J.; Freer, S. T.; Alden, R. A. *J. Biol. Chem.* **1974**, *249*, 6339–6346.
(57) Carter, C. W. *J. Biol. Chem.* **1977**, *252*, 7802–7811.
(58) Chen, K. S.; Jung, Y. S.; Bonagura, C. A.; Tilley, G. J.; Prasad, G. S.; Sridhar, V.; Armstrong, F. A.; Stout, C. D.; Burgess, B. K. *J. Biol. Chem.* **2002**, *277*, 5603–5610.
(59) Heering, H. A.; Bulsink, Y. B. M.; Hagen, W. R.; Meyer, T. E. *Eur. J. Biochem.* **1995**, *232*, 811–817.
(60) Ollagnier, S.; Mulliez, E.; Schmidt, P. P.; Eliasson, R.; Gaillard, J.; Deronzier, C.; Bergman, T.; Graslund, A.; Reichard, P.; Fontecave, M. *J. Biol. Chem.* **1997**, *272*, 24216–24223.
(61) Stubbe, J.; Nocera, D. G.; Yee, C. S.; Chang, M. C. *Chem. Rev.* **2003**, *103*, 2167–201.
(62) Shih, C.; Museth, A. K.; Abrahamsson, M.; Blanco-Rodriguez, A. M.; Di Bilio, A. J.; Sudhamsu, J.; Crane, B. R.; Ronayne, K. L.; Towrie, M.; Vlcek, A., Jr.; Richards, J. H.; Winkler, J. R.; Gray, H. B. *Science* **2008**, *320*, 1760–1762.
(63) Reece, S. Y.; Nocera, D. G. *Annu. Rev. Biochem.* **2009**, *78*, 673–699.
(64) Minnihan, E. C.; Seyedsayamdost, M. R.; Stubbe, J. *Biochemistry* **2009**, *48*, 12125–12132.
(65) Zhang, Y.; Zhu, X.; Torelli, A. T.; Lee, M.; Dzikovski, B.; Koralewski, R. M.; Wang, E.; Freed, J.; Krebs, C.; Ealick, S. E.; Lin, H. *Nature* **2010**, *465*, 891–896.
(66) Kabsch, W. *J. Appl. Crystallogr.* **1993**, *26*, 795–800.
(67) Navaza, J. *Acta Crystallogr., Sect. D: Biol. Crystallogr.* **2001**, *57*, 1367–1372.
(68) De La Fortelle, E.; Irwin, J. J.; Bricogne, G. *Crystallogr. Comput.* **1997**, *7*, 1–9.
(69) Morris, R. J.; Perrakis, A.; Lamzin, V. S. *Macromolecular Crystallography, Part D*; Carter, C. W., Jr., Sweet, R. M., Eds.; Academic Press: New York, 2003; Vol. 374, pp 229−244.
(70) Emsley, P.; Cowtan, K. *Acta Crystallogr., Sect. D: Biol. Crystallogr.* **2004**, *60*, 2126–2132.
(71) Brünger, A. T.; Adams, P. D.; Clore, G. M.; DeLano, W. L.; Gros, P.; Grosse-Kunstleve, R. W.; Jiang, J. S.; Kuszewski, J.; Nilges, M.; Pannu, N. S.; Read, R. J.; Rice, L. M.; Simonson, T.; Warren, G. L. *Acta Crystallogr., Sect.: Biol. Crystallogr.* **1998**, *54*, 905–921.
(72) Adams, P. D.; *et al. Acta Crystallogr., Sect. D: Biol. Crystallogr.* **2010**, *66, 213–221.*
(73) Collaborative Computational Project, Number 4. *Acta Crystallogr., Sect. D: Biol. Crystallogr.* **1994**, *50*, 760−763.
(74) Binkowski, T. A.; Naghibzadeg, S.; Liang, J. *Nucleic Acids Res.* **2003**, *31*, 3352–3355.
(75) Holm, L.; Rosenstrom, P. *Nucleic Acids Res.* **2010**, *38*, 545–549.
(76) Krissinel, E.; Henrick, K. *Acta Crystallogr., Sect. D: Biol. Crystallogr.* **2004**, *60*, 2256–2268.
(77) PyMOL Molecular Graphics System, Version 1.2r3pre, Schrödinger, LLC (access date: 2009).
(78) Ullmann, G. M.; Knapp, E. W. *Eur. Biophys. J.* **1999**, *28*, 533–555.
(79) Bashford, D.; Gerwert, K. *J. Mol. Biol.* **1992**, *224*, 473–486.
(80) MacKerell, A. D.; *et al. J. Phys. Chem. B* **1998**, *102, 3586–3616.*